



저작자표시-비영리-변경금지 2.0 대한민국

이용자는 아래의 조건을 따르는 경우에 한하여 자유롭게

- 이 저작물을 복제, 배포, 전송, 전시, 공연 및 방송할 수 있습니다.

다음과 같은 조건을 따라야 합니다:



저작자표시. 귀하는 원저작자를 표시하여야 합니다.



비영리. 귀하는 이 저작물을 영리 목적으로 이용할 수 없습니다.



변경금지. 귀하는 이 저작물을 개작, 변형 또는 가공할 수 없습니다.

- 귀하는, 이 저작물의 재이용이나 배포의 경우, 이 저작물에 적용된 이용허락조건을 명확하게 나타내어야 합니다.
- 저작권자로부터 별도의 허가를 받으면 이러한 조건들은 적용되지 않습니다.

저작권법에 따른 이용자의 권리는 위의 내용에 의하여 영향을 받지 않습니다.

이것은 [이용허락규약\(Legal Code\)](#)을 이해하기 쉽게 요약한 것입니다.

[Disclaimer](#)



석 사 학 위 논 문

Protective Effects of HDAC6 Inhibitor on Methamphetamine-Induced Neurotoxicity

계 명 대 학 교 대 학 원
의 학 과

HA THI NGOC VY

HA
THI
NGOC
VY
2024
년
8월

지 도 교 수 서 지 혜

2 0 2 4 년 8 월



Protective Effects of HDAC6 Inhibitor on Methamphetamine–Induced Neurotoxicity

지 도 교 수 서 지 혜

이 논문을 석사학위 논문으로 제출함

2 0 2 4 년 8 월

계 명 대 학 교 대 학 원

의학과 생화학 전공

HA THI NGOC VY

HA THI NGOC VY의 석사학위 논문을 인준함

주 심 하 은 영

부 심 서 지 혜

부 심 신 소 진

계 명 대 학 교 대 학 원

2 0 2 4 년 8 월

Acknowledgement

First of all, I sincerely thank my supervisor, Professor Ji Hae Seo, for her dedication and expertise towards this thesis of mine. My thesis would not be done without her advice.

Secondly, I want to express my deepest thanks to Professor Eun Young Ha for allowing me to work in one of the most accommodating laboratories in the lab system of the School of Medicine.

I wish to express my gratitude to all seniors and laboratory members for the cherished time spent together in the laboratory and social settings.

In addition, I also want to dedicate this part to praise all my friends and my family for their encouragement all through my studies.

2024년 8월

HA THI NGOC VY

Table of Contents

1. Introduction	1
2. Materials and Methods	3
3. Results	15
4. Discussion	38
5. Summary	42
References	43
Abstract	53
국문초록	54

List of Table

Table 1. Details of Primer Pair Sequences	14
---	----

List of Figures

Figure 1. Structure of SON-7-108	13
Figure 2. SON-7-108 prevents α -tubulin deacetylation in SH-SY5Y cells	20
Figure 3. SON-7-108 prevents α -tubulin deacetylation in METH-injected mice	21
Figure 4. SON-7-108 prevents METH-induced BBB leakage <i>in vivo</i>	23
Figure 5. SON-7-108 prevents METH-induced cerebrovascular dysfunction in HBMECs	25
Figure 6. SON-7-108 moderates METH-induced neuroinflammation <i>in vivo</i>	27
Figure 7. SON-7-108 moderates METH-induced neuroinflammation <i>in vitro</i>	29
Figure 8. SON-7-108 eliminates METH-induced dopaminergic neuronal damage	31

Figure 9. SON-7-108 reduces METH-induced oxidative stress <i>in vivo</i> ·	33
Figure 10. SON-7-108 reduces ROS generation via prevention of Prx1 deacetylation	35
Figure 11. Summary of the study	37

1. Introduction

Methamphetamine (METH) is a worldwide spreading psychostimulant. Even though METH has been used as a prescribed drug for weight loss and depression in the previous century, it causes highly addictive among users (1). METH abuse reduces the functions of organs, especially the brain. The use of METH exacerbates the immune system of patients with infectious diseases (2-6).

METH, due to its moderate molecular weight, exhibits significant capability to penetrate the blood-brain barrier (BBB) (7). Upon entry into the brain, METH induces hyperthermia and initiates the generation of reactive oxygen species (ROS) within endothelial cells, the key constituents of the BBB. This cascade subsequently triggers neuroinflammatory processes, characterized by the activation of astrocytes and microglia, and an increase in the production of pro-inflammatory cytokines including tumor necrosis factor alpha (TNF- α) and interleukin-1 beta (IL-1 β). Concurrently, METH exposure downregulates expressions of junctional proteins, thereby compromising the integrity of the BBB. These structural and functional perturbations collectively manifest as BBB damage (8-11).

METH also disrupts the dopaminergic neuronal system. After entering dopaminergic cells through dopamine transporters (DAT), METH reduces tyrosine hydroxylase (TH), the crucial enzyme in dopamine (DA) synthesis, and decreases the function of vesicular monoamine transporter 2 (VMAT-2). METH also blocks the reuptake of extracellular DA, thus elevating extracellular DA levels. The metabolism of excess DA results in the increased production of ROS (12,13).

Histone deacetylase 6 (HDAC6) belongs to class IIb of the HDACs

family and is known for catalyzing the deacetylation of lysine residues on histones within chromatin (14). HDACs are categorized into subgroups based on their structural motifs, cellular localization, enzymatic functions, and substrate specificity. HDAC6 stands out due to its dual catalytic domains, which are pivotal for its enzymatic functions. Additionally, HDAC6 possesses a unique ubiquitin-binding zinc-finger domain that facilitates interactions with the ubiquitin-proteasome system, thereby playing a crucial role in protein degradation processes (15–17).

HDAC6 exerts its catalytic function by deacetylating tubulin, a crucial structural protein in microtubules, thereby compromising cytoskeletal stability and morphology. This process subsequently impedes mitochondrial transport. Furthermore, HDAC6 mediates the deacetylation of peroxiredoxins, specifically peroxiredoxin-1 (Prx1) and peroxiredoxin-2 (Prx2) (18). Elevated HDAC6 activity has been implicated in exacerbating neurodegenerative disorders such as Parkinson's disease, Huntington's disease, and Alzheimer's disease. Therefore, the use of selective HDAC6 inhibitors, such as tubacin, tubastatin A (Tub A), and ACY-1215, offers potential therapeutic relief from these conditions (19–21).

Recently, numerous HDAC6 inhibitors have been investigated to find therapeutic candidates for neurodegenerative diseases (22–25). Benzimidazole is proclaimed for its high permeability through the BBB (26), proposing SON-7-108, a benzimidazole-based HDAC6 inhibitor, as a promising candidate for effective HDAC6 inhibition with high BBB permeability.

The objective of this study is to evaluate the efficacy of SON-7-108 in inhibiting HDAC6 activity and its potential to mitigate METH-induced BBB disruption and neurotoxicity, employing both *in vitro* and *in vivo* experimental paradigms.

2. Materials and Methods

2.1. Cell culture:

Human neuroblastoma cell line, SH-SY5Y, and C57BL/6 murine-derived microglial cell line, BV2, were grown in Dulbecco's modified eagle medium (DMEM) supplementing with 10% fetal bovine serum (FBS) (Welgene, Gyeongsangbuk-do, Korea), and 1% penicillin/streptomycin at 37 °C in a 5% CO₂ moisturized environment. The human brain microvascular endothelial cells (HBMECs) were maintained in an endothelial cell growth medium (EGM-2) (Lonza, Walkersville, MD, USA) on the Collagen I (Corning, Bedford, MA, USA) coated dish.

2.2. Compounds synthesis:

SON-7-108 is a novel benzimidazole-based HDAC6 inhibitor. It was synthesized by Professor Young Ho Seo, College of Pharmacy, Keimyung University, Daegu, Republic of Korea.

2.3. Cell viability:

After seeding in 96-well plates with 1×10^3 cells per well, SH-SY5Y cells were treated with SON-7-108 at different concentrations (0, 0.1, 0.25, 0.5, 1, 2.5, 5, and 10 μ M) for 24 hours. Cell viability was checked using cell counting kit-8 (CCK-8) (Dojindo, Kumamoto, Japan) according

to the instructions of the manufacturer. Briefly, cells were incubated with DMEM containing 10% CCK-8 at 37 °C in 5% CO₂ for 1 hour. Absorbance was measured at 450 nm using a microplate reader (SPECTROstar^{nano}, BMG labtech, Germany). The cell viability was expressed as a percentage of the control.

2.4. Western blot analysis of cell lysates:

SH-SY5Y cells were plated in 6-well plates (1.5 x 10⁵ cells per well) and treated with SON-7-108 and other HDAC6 inhibitors, including Tub A and suberoylanilide hydroxamic acid (SAHA) at different concentrations for 24 hours. In addition, SH-SY5Y cells were pretreated with SON-7-108 for 2 hours and exposed to 1 mM METH for 24 hours. The cells were harvested and lysed with radioimmunoprecipitation assay (RIPA) buffer (Elpis Bio, Daejeon, Korea) containing 2 μM phenylmethylsulphonyl fluoride (PMSF) (Cell Signaling Technology, Beverly, MA, USA) and 1% protease inhibitor (PI) (Gendepot, Katy, TX, USA). The lysates were centrifuged at 13,000 g at 4 °C for 20 minutes. Subsequently, the supernatant was transferred to new prechilled tubes and protein quantification was carried out utilizing the bicinchoninic acid (BCA) protein assay kit (Thermo Fisher Scientific, MA, USA). Then, 30 μg of protein was analyzed using sodium dodecyl sulfate-polyacrylamide gel electrophoresis (SDS-PAGE). Protein was then transferred to the nitrocellulose membrane (GE Health Care, IL, USA). Next, the membranes were blocked with 5% skim milk in tris-buffered saline containing tween 20 (TBS-T) at room temperature for 30 minutes. The membranes were then incubated with anti-α-tubulin, anti-histone H3, anti-acetyl histone H3 (1:1,000 dilution, Cell Signaling Technology,

Beverly, MA, USA), anti-acetyl- α -tubulin, anti-HDAC6 (1:1,000 dilution, Santa Cruz Biotechnology, TX, USA), and anti-GAPDH (1:3,000 dilution, Promega Corporation, WI, USA) primary antibodies at 4 °C overnight. Later, the membranes were washed with TBS-T 3 times for 10 minutes each and then incubated with horseradish peroxidase (HRP)-conjugated secondary anti-mouse IgG or anti-rabbit IgG antibodies (1:10,000 dilution, Cell Signaling Technology, Beverly, MA, USA). Protein was then detected using EZ-Western Lumi Pico Kit reagent (Dogen, Seoul, Korea) in Gel Doc XR+ Gel Documentation System (Bio-Rad, CA, USA).

2.5. Animals and methamphetamine-induced injury model:

The experiments were performed on 7-week-old male C57BL/6J mice purchased from Hyo-Chang Science (Daegu, Korea). The mice were maintained at a control temperature (24 ± 1 °C), humidity, and lighting (12:12 hours light-dark cycle). After 1 week of acclimatization, the mice were divided into 4 groups: Control (CON), METH, METH + SON-7-108, and SON-7-108. To investigate the effects of SON-7-108 on BBB leakage, mice were intraperitoneally injected (i.p.) with a single dosage of 10 mg/kg SON-7-108 or 5% dimethyl sulfoxide (DMSO) in saline 2 hours before 4 administrations of METH at 10 mg/kg every 2 hours. The mice were anesthetized, and brains were collected 2 hours after the last administration of METH. To investigate the effects of SON-7-108 on METH-induced neurotoxicity *in vivo*, mice were i.p. injected with a single dose of 10 mg/kg SON-7-108 or 5% DMSO in saline daily. Two hours after the first injection of SON-7-108, mice

were injected with 4 administrations of METH at 10 mg/kg every 2 hours. Seventy-two hours after the last injection of METH, the mice were then anesthetized and perfused with cold phosphate-buffered saline (PBS) containing 100 U/mL heparin. The brain was then sliced horizontally, and a hemisphere was stored at -80 °C while another was snap-frozen in optimal cutting temperature (OCT) compound (Sakura Finetek USA, CA, USA). This study (KM-2023-04) was acclaimed by the Institutional Animal Care and Use Committee (IACUC) of Keimyung University, School of Medicine.

2.6. Western blot analysis of brain tissues:

T-PER Tissue Protein Extraction Reagent buffer (Thermo Fisher Scientific, MA, USA) containing 2 μ M PMSF and 1% PI (Gendepot, Katy, TX, USA) was employed to homogenize brain tissues. The lysates were centrifuged at 13,000 g at 4 °C for 20 minutes. The supernatant was transferred to new prechilled tubes and protein quantification was carried out using the BCA protein assay kit (Thermo Fisher Scientific, MA, USA). Then, 20 μ g of protein was analyzed using SDS-PAGE before being transferred to the nitrocellulose membrane. Next, the membranes were blocked with 5% skim milk in TBS-T at room temperature for 30 minutes. The membranes were then incubated with anti- α -tubulin (1:1,000 dilution, Cell Signaling Technology, Beverly, MA, USA), anti-acetyl- α -tubulin (1:1,000 dilution, Santa Cruz Biotechnology, TX, USA), anti-glial fibrillary acidic protein (GFAP) (1:1,000 dilution, Cell Signaling Technology, Beverly, MA, USA), anti-TH (1:200 dilution, Invitrogen, Thermo Fisher Scientific, MA, USA), anti-DAT (1:1,000 dilution, Proteintech Group, IL, USA), and anti-GAPDH (1:3,000 dilution,

Promega Corporation, WI, USA) primary antibodies at 4 °C overnight. Later, the membranes were washed with TBS-T 3 times for 10 minutes each and incubated with HRP-conjugated secondary anti-mouse IgG or anti-rabbit IgG antibodies (1:10,000 dilution, Cell Signaling Technology, Beverly, MA, USA). Protein was detected using Lumi-Pico reagent in Gel Doc XR+ Gel Documentation System (Bio-Rad, CA, USA).

2.7. Immunohistochemistry (IHC) analysis:

The 10 μ m sections from OCT-embedded tissues were obtained using cryostat microtome SLEE medical GmbH (Olm, Germany). Tissue sections were fixed with cold methanol, or 4% paraformaldehyde (PFA) for 10 minutes before being incubated with PBS containing glycine solution. After washing with PBS, slides were quenched with 0.3% hydroxy peroxide solution for 15 minutes before being blocked with blocking solution (3% goat serum in PBS containing 2% skim milk). Tissue sections were incubated with primary antibodies, including anti-acetyl- α -tubulin, (1:1,000 dilution, Cell Signaling Technology, Beverly, MA, USA), anti-TH (1:200 dilution, Invitrogen, Thermo Fisher Scientific, MA, USA), anti-8-hydroxy-2'-deoxyguanosine (8-OHdG) (1:50 dilution, Santa Cruz Biotechnology, TX, USA), anti-4-hydroxynonenal (4-HNE) (1:50 dilution, R&D Systems, MN, USA), anti-DAT (1:100 dilution, Proteintech Group, IL, USA), anti-Iba1 (1:100 dilution, FUJIFILM Wako Pure Chemical Corporation, Osaka, Japan), anti-IL-1 β , and anti-neutrophil elastase (1:100 dilution, Abcam, Cambridge, UK) antibodies at 4 °C overnight. After being rinsed with PBS, the sections were incubated with the interrelated HRP-secondary antibodies at room temperature for 1 hour before being visualized with

the 3,3'-diaminobenzidine (DAB) substrate kit (Vector Laboratories, Burlingame, CA, USA). To detect IgG, sections were incubated with anti-mouse IgG antibody (1:100 dilution, Cell Signaling Technology, Beverly, MA, USA) at room temperature for 1 hour and visualized using DAB. The sections were then counterstained with hematoxylin (Dako, Glostrup, Denmark). Stained sections were captured using a light microscope (DM750, Leica, Wetzlar, Germany) and quantified using Image J (National Institutes of Health, Bethesda, MD, USA).

2.8. Transendothelial electrical resistance (TEER) measurement and fluorescein isothiocyanate-dextran (FITC-dextran) permeability assay:

HBMECs were plated on the collagen-coated insert of the transwells (Corning, Bedford, MA, USA) and grown until reaching 100% confluence. The cells were next pretreated with SON-7-108 at 10 μ M for 2 hours before the 24-hour treatment with METH at 1 mM. Then, the TEER values were measured by STX2/chopstick electrodes connected to EVOM2 (World Precision Instruments, Sarasota, USA) to calculate the unit area resistance. After that, the cells were incubated with 10 μ g/mL of FITC-dextran (70 kDa, Sigma-Aldrich, MA, USA) for 2 hours. Then, 100 μ L media from the basolateral compartment was measured for the fluorescent intensity that excited at 485 nm and emitted at 535 nm by a microplate reader (Infinite M200 Pro, Tecan, Mannedorf, Switzerland).

2.9. Immunofluorescent (IF) analysis:

Brain sections were fixed with cold 4% PFA for 10 minutes followed by washing with PBS before being blocked with blocking solution for 30 minutes. The slides were then incubated with primary anti-GFAP antibody (1:100 dilution, Cell Signaling Technology, Beverly, MA, USA) at 4 °C overnight. Following this, the sections were washed with PBS 3 times for 10 minutes each before being incubated with secondary goat anti-mouse IgG Alexa Fluor 488 antibody (1:1,000 dilution, Thermo Fisher Scientific, MA, USA) at room temperature for 1 hour. The sections were washed with PBS and counterstained with 4',6-diamidino-2-phenylindole (DAPI) (1:100 dilution, Invitrogen, Thermo Fisher Scientific, MA, USA) for 10 minutes. The residues of DAPI were washed with PBS several times before being mounted using Prolong Gold Antifade Mountant (Invitrogen, Thermo Fisher Scientific, MA, USA). Signals were captured by a confocal laser microscope (Carl Zeiss LSM5 EX CITER, Jena, Germany).

2.10. Immunocytochemistry (ICC) analysis:

HBMECs were seeded on collagen-coated coverslips, while BV2 cells were seeded on the coverslips. The cells were pretreated with SON-7-108 2 hours before treatment with METH for 24 hours. These cells were fixed with 4% PFA at room temperature for 15 minutes. Cells were next incubated with 0.1% Triton X-100 in PBS at room temperature for 10 minutes and blocked with 1% BSA in PBS-T for 30 minutes. Cells were incubated with primary antibodies, including anti-zonula occludens-1 (ZO-1) (1:100 dilution, Invitrogen, Thermo Fisher Scientific, MA, USA), anti-vascular endothelial-cadherin (VE-Cadherin) (1:200 dilution, Abcam, Cambridge, UK), and anti-Iba1

(1:100 dilution, FUJIFILM Wako Pure Chemical Corporation, Osaka, Japan) antibodies at 4 °C overnight. To observe the filamentous actin (F-Actin), HBMECs were incubated with Phalloidin-iFluor 488 reagent (1:1,000 dilution, Abcam, Cambridge, UK) at room temperature for 1 hour. The cells were incubated with secondary goat anti-mouse IgG Alexa Fluor 488 or goat anti-rabbit IgG Alexa Fluor 488 and 568 (1:500 dilution, Thermo Fisher Scientific, MA, USA) antibodies and counterstained with DAPI (1:100 dilution, Invitrogen, Thermo Fisher Scientific, MA, USA) at room temperature for 10 minutes. The pictures were captured using the confocal laser microscope (Leica, Wetzlar, Germany).

2.11. Quantitative real time-polymerase chain reaction (qRT-PCR):

SH-SY5Y cells (1.5×10^5 cells per well) and BV2 cells (2×10^5 cells per well) were placed in 6-well plates. The cells were pretreated with SON-7-108 at different concentrations (1, 5, or 10 μ M) for 2 hours before being treated with METH at 1 mM for 24 hours. The total RNA was extracted from cells by using Trizol reagent (Invitrogen, Thermo Fisher Scientific, MA, USA) according to the instructions of manufacturer. The purity and concentration of RNA were measured by NanoDrop 2000 spectrophotometer (NanoDrop Technologies, Wilmington, DE, USA). Complementary DNA (cDNA), reverse transcribed from 3 μ g RNA using Moloney Murine Leukemia Virus (M-MLV) reverse transcriptase (Promega, WI, USA) according to the instructions of manufacturer. For qRT-PCR, cDNA was performed with SYBR Green PCR Master Mix (Toyobo, Osaka, Japan) using a LightCycler 480

(Roche, Basel, Switzerland). The comparative Ct ($2^{-\Delta\Delta Ct}$) method was used for mRNA level quantification after normalizing to the level of housekeeping gene β -actin. Primer sequences as listed in Table 1.

2.12. ROS detection:

To detect superoxide anion in METH-induced BBB leakage mice, dihydroethidium (DHE) (Thermo Fisher Scientific, MA, USA) reagent was utilized. Brain sections were stained with 10 μ M DHE under warm conditions for 30 minutes and washed with PBS several times. The signals were examined by fluorescent microscope (Axio Observer A1, Carl Zeiss, Jena, Germany) and quantified using Image J software (National Institutes of Health, Bethesda, MD, USA).

For SH-SY5Y cells, BV2 cells (1.5×10^5 cells per well), and HBMECs (1×10^5 cells per well) were placed in 12-well plates. The cells were pretreated with SON-7-108 at different concentrations (1, 5, and 10 μ M) for 2 hours and exposed to 1 mM METH for 30 minutes. Next, cells were washed with PBS and incubated with 30 μ M 2',7'-dichlorodihydrofluorescein diacetate (DCF-DA) at 37 °C for 30 minutes in a 5% CO₂ humidified environment. Then, cells were washed with PBS and signals were obtained after 1 minute of exposure to the green fluorescence using fluorescent microscopy (CKX53, Olympus, Tokyo, Japan). Figures were quantified using Image J software.

2.13. Immunoprecipitation (IP) assay:

After pretreatment with 10 μ M SON-7-108 for 2 hours, SH-SY5Y

cells were treated with 1 mM METH for 30 minutes. Cells were next lysed with RIPA buffer containing 2 μ M PMSF and 1% PI, and protein quantification was carried out as mentioned before. The whole lysate protein was incubated with protein A-Agarose (Santa Cruz Biotechnology, TX, USA) conjugated with anti-acetylated lysine antibody (1:1,000 dilution, Cell Signaling Technology, Beverly, MA, USA) at 4 °C overnight. The complex was washed with a washing buffer containing 20 mM Tris (pH 8.0), 150 mM NaCl, 0.2 mM EDTA, and 0.1% Triton X-100 and analyzed by SDS-PAGE before being transferred to the nitrocellulose membrane. The membranes were incubated with anti-Prx-1 antibody (1:1,000 dilution, Invitrogen, Thermo Fisher Scientific, MA, USA) and anti-GAPDH (1:3,000 dilution, Promega Corporation, WI, USA) primary antibodies before being incubated with HRP-conjugated secondary anti-mouse IgG or anti-rabbit IgG antibodies (1:10,000 dilution, Cell Signaling Technology, Beverly, MA, USA). Protein was detected using Lumi-Pico reagent in Gel Doc XR+ Gel Documentation System.

2.14. Statistical analysis:

Experiments were repeated at least three times to gain consistent results. The results were indicated as mean \pm standard deviation. Statistical analysis was performed using a student's *t*-test and *p* value of < 0.05 was considered to indicate statistical significance.

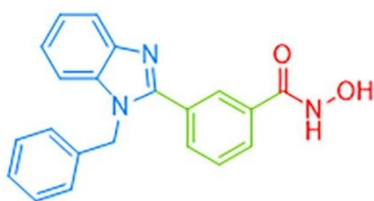


Figure 1. Structure of SON-7-108. This benzimidazole-based compound is synthesized by Professor Young Ho Seo, College of Pharmacy, Keimyung University, Daegu, Republic of Korea.

Table 1. Details of Primer Pair Sequences

Species	Name	Sequences of primers
Human	β -actin	Forward: 5'-GGACTTCGAGCAAGAGATGG-3'
		Reverse: 5'-AGCACTGTGTTGGCGTSCAG-3'
	TNF- α	Forward: 5'-TCCTTCAGACACCCTCAACC-3'
		Reverse: 5'-AGGCCCCAGTTTGAATTCTT-3'
	IL-1 β	Forward: 5'-CTGTCCTGCGTGTTGAAAGA-3'
		Reverse: 5'-TTGGGTAATTTTTGGGATCT-3'
Mouse	β -actin	Forward: 5'-AGCCATGTACGTAGCCATCC-3'
		Reverse: 5'-TTTCCCTCTCAGCTGTGGTG-3'
	TNF- α	Forward: 5' -GGCCTCTCTACCTTGTTGCC-3'
		Reverse: 5' -CAGCCTGGTCACCAAATCAG-3'
	IL-1 β	Forward: 5' - GCCCATCCTCTGTGACTCAT-3'
		Reverse: 5' - AGGCCACAGGTATTTTGTCTG - 3'

IL-1 β : interleukin1-beta; TNF- α : tumor necrosis factor alpha

3. Results

3.1. Inhibition of HDAC6 activity by SON-7-108 *in vitro*:

To determine the effect of SON-7-108 on HDAC6 activity *in vitro*, SH-SY5Y cells were treated with SON-7-108 at different concentrations for 24 hours. Cell viability was evaluated using the CCK-8 kit, revealing no significant decrease in cell viability at concentrations up to 10 μ M (Figure 2A). The western blot result indicated that SON-7-108 selectively increased the acetyl- α -tubulin (substrate of HDAC6) while showing no impact on acetyl-histones H3 (substrate of HDAC1) (Figure 2B). In comparison to Tub A and SAHA at equivalent concentrations, SON-7-108 showed similar results to these reference compounds (Figure 2C). Additionally, western blot showed that pretreatment with SON-7-108 at 3 different concentrations (1, 5, or 10 μ M) reduced METH-induced deacetylation of α -tubulin (Figure 2D). These results suggest that SON-7-108 selectively inhibits HDAC6 activity.

3.2. Inhibition of HDAC6 activity by SON-7-108 *in vivo*:

SON-7-108 was further examined for its effect on HDAC6 activity *in vivo* according to the scheme mentioned in Figure 3A. Seventy-two hours after the last injection of 10 mg/kg METH, mice were anesthetized and their striatal regions were analyzed using western blot, revealing that METH reduced the acetyl- α -tubulin level. However,

pretreatment with SON-7-108 effectively reduced METH-induced deacetylation of α -tubulin as demonstrated in Figure 3B. This was confirmed by IHC images (Figure 3C), which displayed a consistent pattern. These results confirm the HDAC6 inhibition of SON-7-108 *in vitro* and *in vivo*.

3.3. Protective effect of SON-7-108 against BBB leakage in METH-injected mice:

Next, to investigate the protective effect of SON-7-108 on METH-induced neurotoxicity, BBB permeability was assessed following the experimental scheme demonstrated in Figure 4A. The IHC analysis showed significantly increased IgG signals in the hippocampus and striatum regions of METH-injected mice, approximately 15 times and 12 times higher than those in the control group, respectively. Pretreatment with SON-7-108 mitigated these effects of METH, as evidenced by the reduced IgG signals shown in Figure 4B. Furthermore, SON-7-108 pretreatment also attenuated the METH-induced neutrophil infiltration, as displayed in Figure 4C. These results suggest that SON-7-108 reduces METH-induced BBB dysfunction in the hippocampus and striatum regions.

3.4. Protective effect of SON-7-108 against METH-induced cerebrovascular dysfunction in HBMECs:

The activity of SON-7-108 in mitigating cerebrovascular dysfunction

was accessed using HBMECs. By utilizing the EVOM2 device, the low TEER value caused by METH-reduced the cell monolayer integrity observed, but pretreatment with SON-7-108 counteracted this action of METH (Figure 5A). In Figure 5B, an increased fluorescent intensity of FITC-dextran caused by METH-induced paracellular permeability was attenuated by SON-7-108 pretreatment. METH also induced the redistribution of junctional proteins and increased formation of F-Actin, as shown in Figure 5C. However, these changes were reduced by pretreatment with SON-7-108. These results suggest that SON-7-108 prevents METH-induced cerebrovascular dysfunction in HBMECs.

3.5. Protective effect of SON-7-108 on neuroinflammation *in vivo*:

The mice were treated as demonstrated in Figure 3A to assess the preventive effect of SON-7-108 on neuroinflammation. In both western blot and IHC results, high expression of GFAP was observed in METH-injected mice, while this phenomenon was alleviated by pretreatment with SON-7-108 (Figure 6A&B). METH also enhanced expressions of IL-1 β and Iba1, which was then diminished by the presence of SON-7-108, suggesting that SON-7-108 reduces METH-induced neuroinflammation *in vivo* (Figure 6C&D).

3.6. Protective effect of SON-7-108 on neuroinflammation *in vitro*:

The effect of SON-7-108 on neuroinflammation *in vitro* was carried

out using BV2 cells. In Figure 7A, pretreatment with SON-7-108 alleviated METH-induced Iba1 expression in BV2 cells. Furthermore, pretreatment of SON-7-108 reduced the mRNA expression levels of TNF- α and IL-1 β in METH-exposed SH-SY5Y (Figure 7B) and BV2 cells (Figure 7C). These results suggest that SON-7-108 downregulates METH-induced neuroinflammation *in vitro*.

3.7. Protective effect of SON-7-108 against METH-induced dopaminergic neuronal damage:

Next, the effect of SON-7-108 on METH-induced dopaminergic neuronal damage was assessed by analyzing expression levels of TH and DAT in brain tissue from METH-injected mice. Both western blot and IHC analyses indicated that pretreatment with SON-7-108 prevented the METH-induced decrease in TH levels (Figure 8A&B). Moreover, pretreatment with SON-7-108 also restored the DAT levels that were abolished by METH (Figure 8C&D). These results provide evidence that SON-7-108 eliminates METH-induced dopaminergic neuronal damage.

3.8. Inhibitory effect of SON-7-108 on oxidative stress *in vivo*:

Next, the inhibitory effect of SON-7-108 on METH-induced oxidative stress *in vivo* was investigated. Two hours after the last administration of METH, ROS production in mice was evaluated using DHE staining. High DHE staining signals, presenting high superoxide anion levels, were observed in the cortex and striatal regions of METH-injected mice. This phenomenon was eliminated by pretreatment of SON-7-108

(Figure 9A). In addition, Figure 9B&C showed that pretreatment with SON-7-108 also reduced levels of 4-HNE (a marker of lipid oxidation products) and 8-OHdG (a marker of DNA damage) enhanced by METH. These results indicate that SON-7-108 reduces METH-induced oxidative stress *in vivo*.

3.9. Inhibitory effect of SON-7-108 on ROS generation by regulating Prx1 deacetylation:

The ROS generation in METH-exposed cells was investigated using DCF-DA. As shown in Figure 10A, DCF-DA signals were enhanced in three types of cells (SH-SY5Y, BV2, and HBMECs) exposed to METH, indicating increased ROS generation. However, pretreatment with SON-7-108 reduced these increases. Prx1 is known as a substrate of HDAC6, and its function is modulated by HDAC6-mediated deacetylation. The acetylated form of Prx1 was evaluated through immunoprecipitation. As a result, pretreatment with SON-7-108 prevented METH-induced deacetylation of Prx1 (Figure 10B).

In conclusion, exposure to METH upregulates HDAC6 activity, which in turn leads to the deacetylation of Prx1. This process enhances the generation of ROS leading to BBB leakage, the initiation of neuroinflammation, and subsequent dopaminergic neuronal damage. Treatment of SON-7-108 prevents the upregulation of HDAC6 activity induced by METH, thereby protecting against METH-induced neurotoxicity (Figure 11).

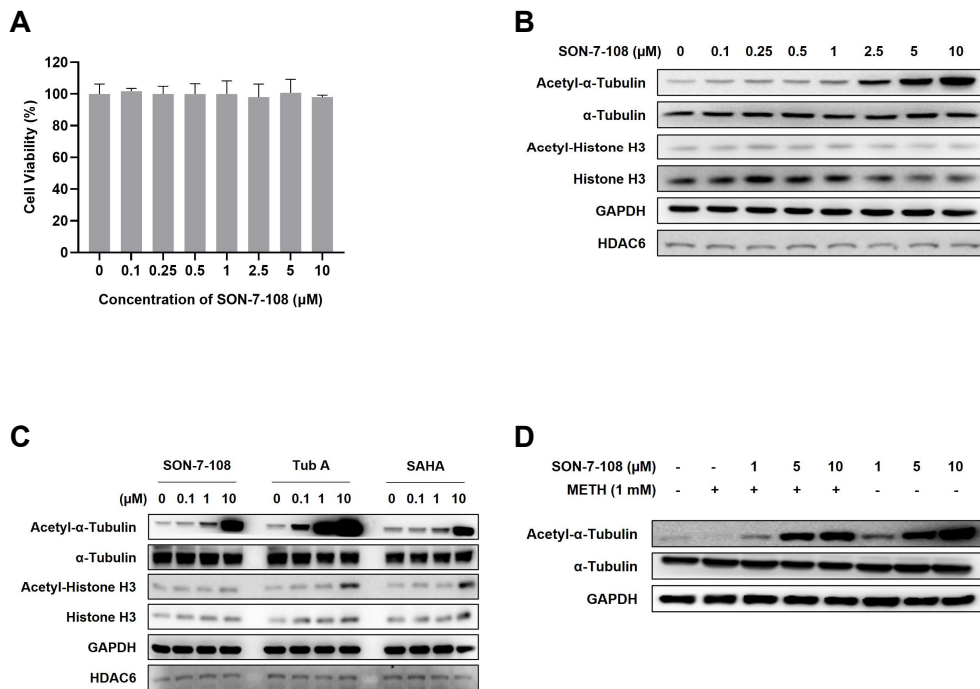
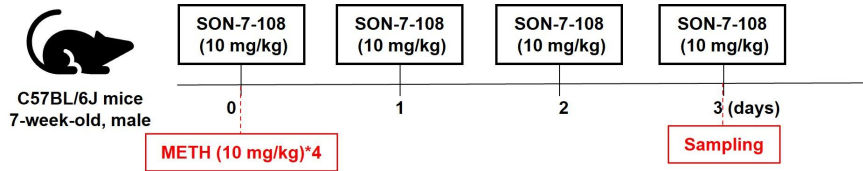
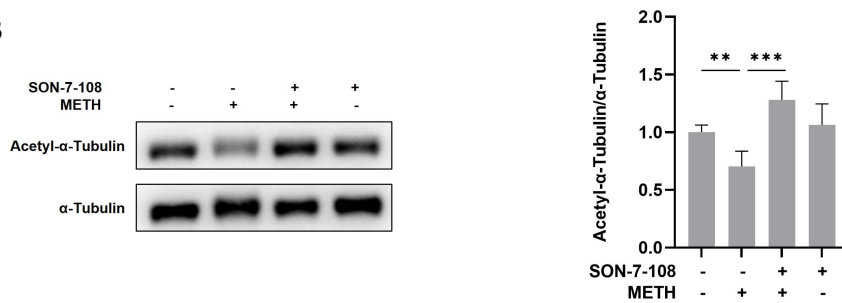


Figure 2. SON-7-108 prevents α -tubulin deacetylation in SH-SY5Y cells. (A) Cell viability of SH-SY5Y cells after 24 hours treatment with SON-7-108. (B) Western blot analysis of α -tubulin and histone H3 acetylation levels. (C) Western blot analysis showing α -tubulin acetylation in SH-SY5Y cells treated with SON-7-108, Tub A, and SAHA at different concentrations. (D) Western blot analysis of α -tubulin acetylation in SH-SY5Y cells pretreated with SON-7-108 and exposed to METH. Data is indicated as mean \pm standard deviation (n=3). HDAC6: histone deacetylase 6; Tub A: tubastatin A; SAHA: suberoylanilide hydroxamic acid; METH: methamphetamine.

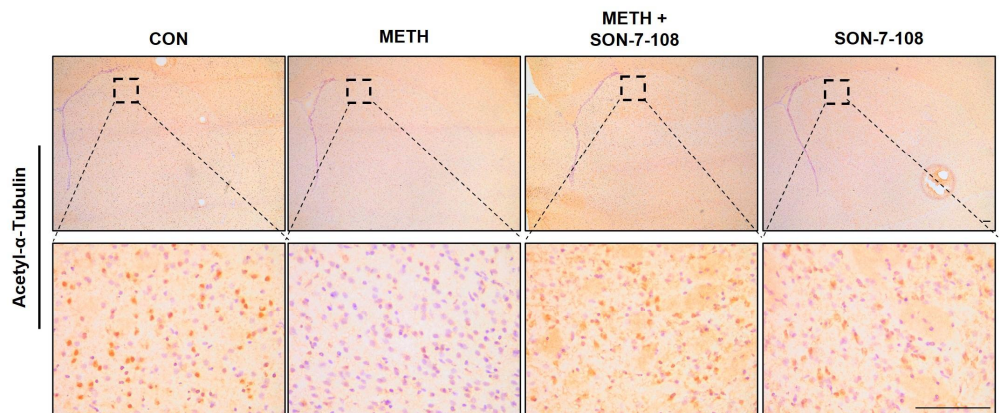
A



B



C



* Scale bar: 100 μm

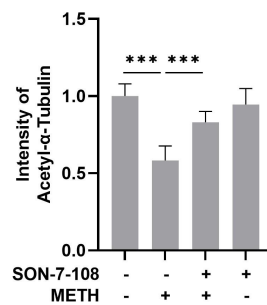
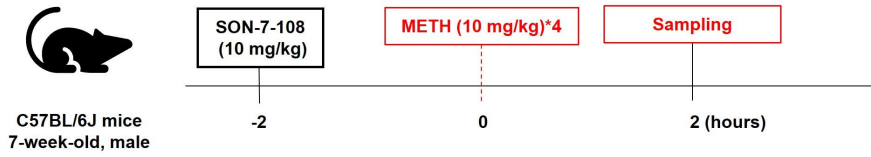
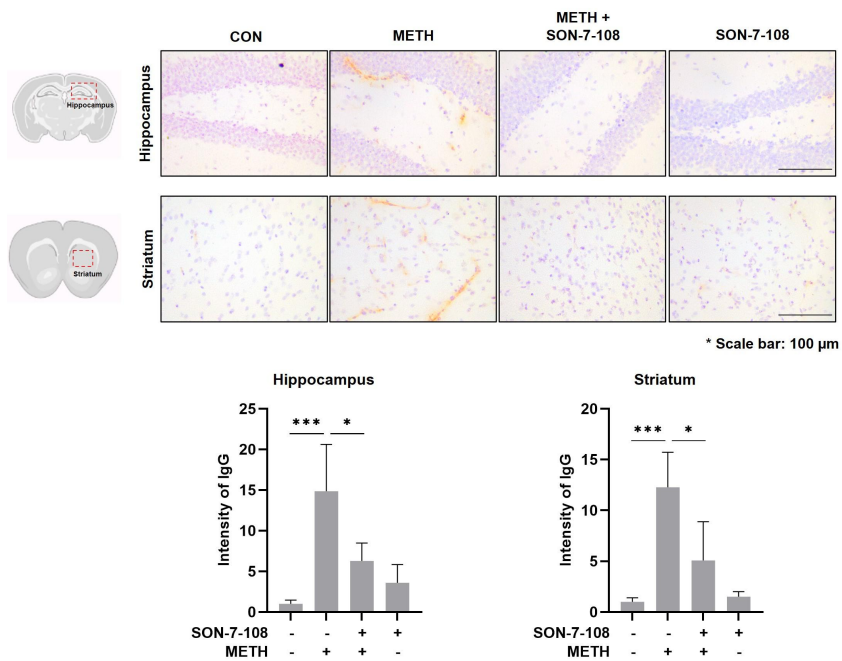


Figure 3. SON-7-108 prevents α -tubulin deacetylation in METH-injected mice. (A) Schematic representation of the *in vivo* experiment conducted on acutely METH-injected mice. (B) Western blot analysis showing the effect of pretreatment with SON-7-108 on METH-injected mice and the quantification of acetyl- α -tubulin level normalized to the level of α -tubulin. (C) IHC images of acetyl- α -tubulin in the striatum region of METH-injected mice were observed under a light microscope and quantified using Image J. Scale bar, 100 μ m. Data is indicated as mean \pm standard deviation (n=5). **: $p < 0.01$, ***: $p < 0.001$. METH: methamphetamine; IHC: immunohistochemistry; CON: control.

A



B



C

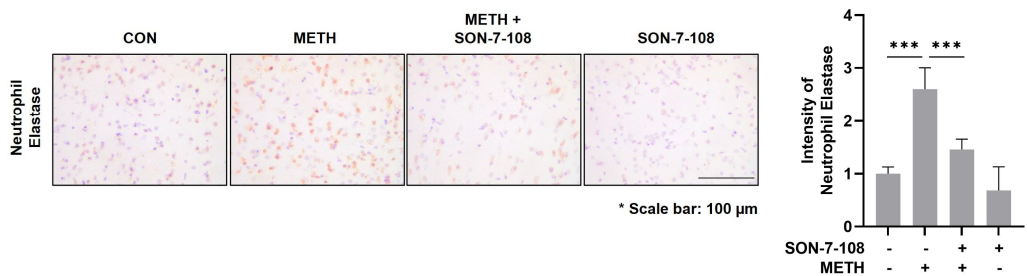


Figure 4. SON-7-108 prevents METH-induced BBB leakage *in vivo*. (A) Illustrative diagram of the *in vivo* experiment for METH-induced BBB leakage. (B) IgG signals in the hippocampus and striatum regions were captured using a light microscope and quantified by Image J. (C) Neutrophil elastase signals in the striatum region were captured using a light microscope and quantified by Image J. Scale bar, 100 μm . Data is indicated as mean \pm standard deviation (n=5). *: $p < 0.05$, ***: $p < 0.001$. IHC: immunohistochemistry; IgG: immunoglobulin G; METH: methamphetamine; CON: control.

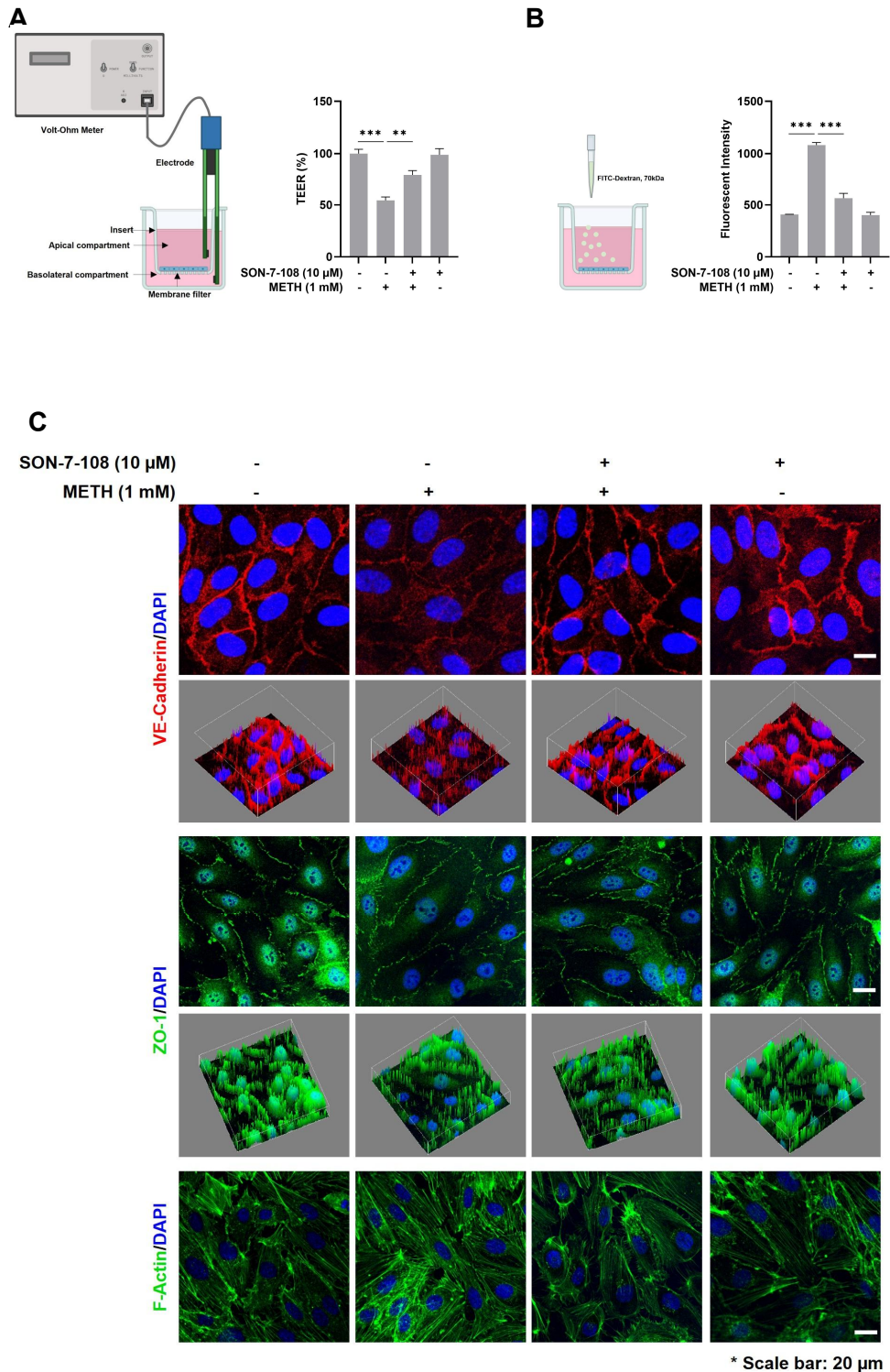
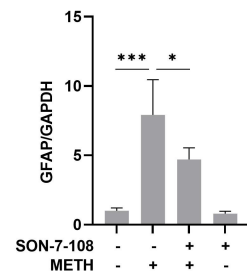
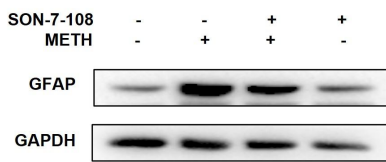
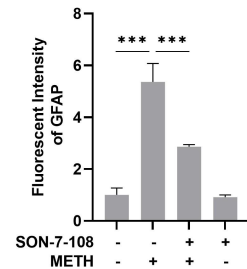
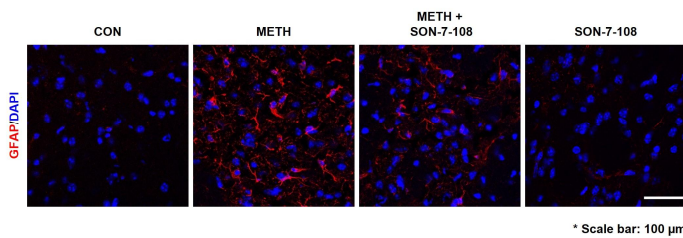


Figure 5. SON-7-108 prevents METH-induced cerebrovascular dysfunction in HBMECs. The HBMECs were pretreated with 10 μ M SON-7-108 for 2 hours and exposed to METH. (A) TEER values of monolayer integrity were measured by STX2/chopstick electrodes connected to EVOM2. (B) Endothelial monolayer permeability was determined by the fluorescent intensity of FITC-dextran. (C) Fluorescent images VE-Cadherin (red signals), ZO-1(green signals), and F-Actin (green signals) were captured by a confocal laser microscope and converted into three-dimensional plot images (applied to localization of junctional proteins) by Image J. Scale bar, 20 μ m. The diagrams were created with BioRender.com. Data is indicated as mean \pm standard deviation (n=3). **: $p < 0.01$, ***: $p < 0.001$. METH: methamphetamine; TEER: transendothelial electrical resistance; FITC-dextran: Fluorescein Isothiocyanate-Dextran; ZO-1: zonula occludens-1; VE-Cadherin: vascular endothelial-cadherin; F-Actin: filamentous actin.

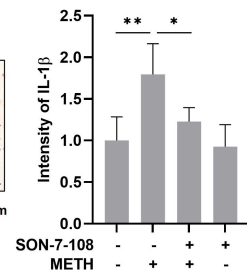
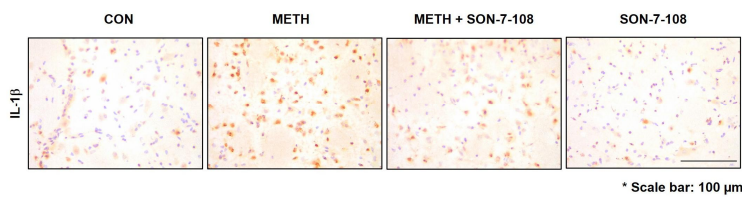
A



B



C



D

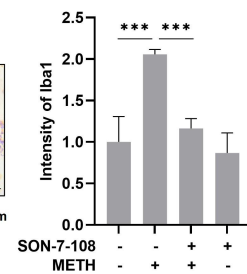
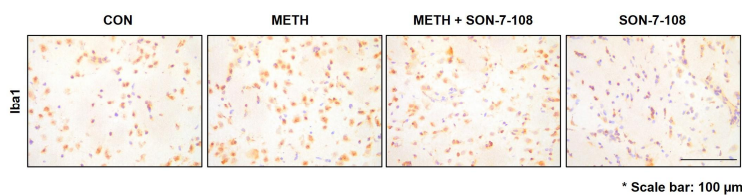
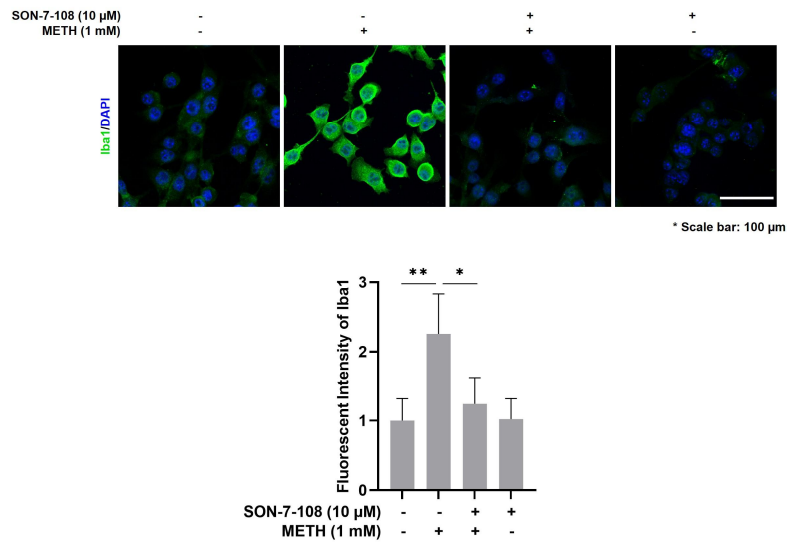
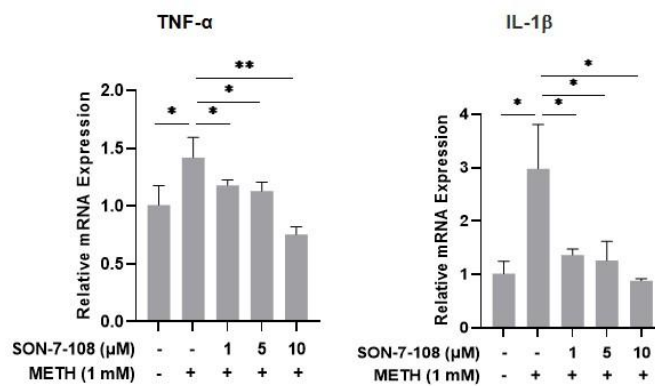


Figure 6. SON-7-108 moderates METH-induced neuroinflammation *in vivo*. Mice were daily intraperitoneally injected with a single dose of 10 mg/kg SON-7-108, and 2 hours after that, mice were injected with 4 administrations of METH at 10 mg/kg every 2 hours. Mice were sacrificed 72 hours after the last injection of METH and striatum sections were used to analyze. (A) Western blot analysis of GFAP, astrocyte activation marker, and the quantification normalized to the level of GAPDH. (B) Fluorescent images of GFAP were captured using a confocal laser microscope and quantified using Image J. (C) IHC images of pro-inflammatory cytokine IL-1 β signals were obtained from a light microscope (original magnification x 40) and the quantification by Image J. (D) IHC images of the Iba1 were obtained from a light microscope and quantified by Image J. Scale bar, 100 μ m. Data is indicated as mean \pm standard deviation (n=5). *: $p < 0.05$, **: $p < 0.01$, ***: $p < 0.001$. METH: methamphetamine; GFAP: glial fibrillary acidic protein; IHC: immunohistochemistry; IL-1 β : interleukin-1 beta; Iba1: ionized calcium-binding adaptor molecule 1; CON: control.

A



B



C

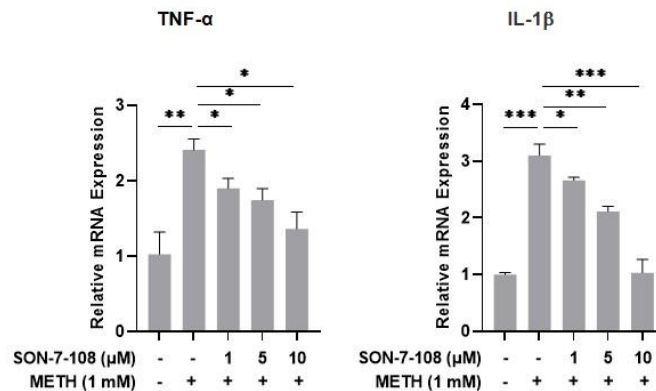
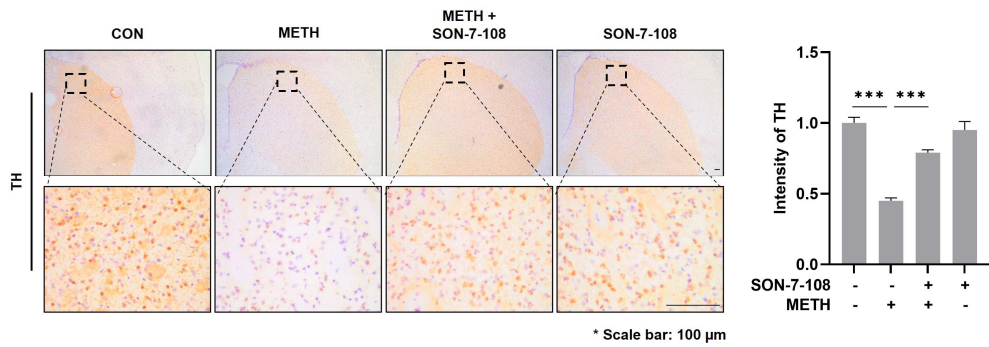


Figure 7. SON-7-108 moderates METH-induced neuroinflammation *in vitro*. SH-SY5Y and BV2 cells were pretreated with different concentrations of SON-7-108 (1, 5, or 10 μ M) for 2 hours and exposed to METH. (A) Fluorescent images of Iba1 in BV2 cells were obtained from a confocal laser microscope and quantified by Image J. Scale bar, 100 μ m. (B) mRNA expressions of pro-inflammatory cytokines, TNF- α and IL-1 β in SH-SY5Y cells. (C) mRNA expressions of pro-inflammatory cytokines, TNF- α and IL-1 β in BV2 cells. Data is indicated as mean \pm standard deviation (n=3). *: $p < 0.05$ **: $p < 0.01$, ***: $p < 0.001$. METH: methamphetamine; Iba1: ionized calcium-binding adaptor molecule 1; TNF- α : tumor necrosis factor alpha; IL-1 β : interleukin-1 beta.

A



B



C



D

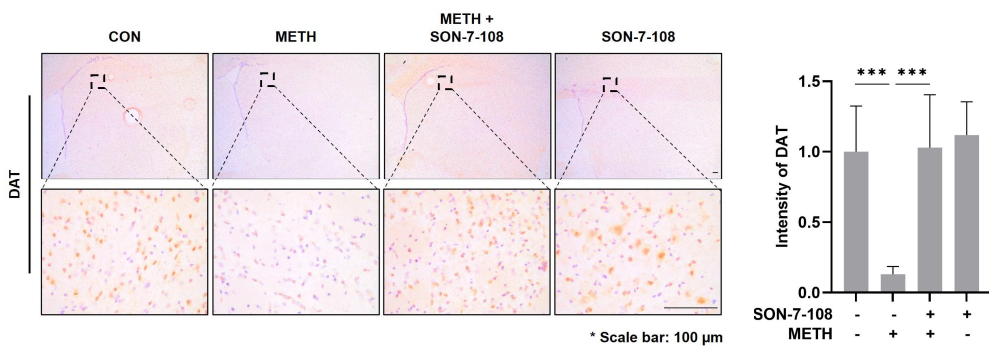
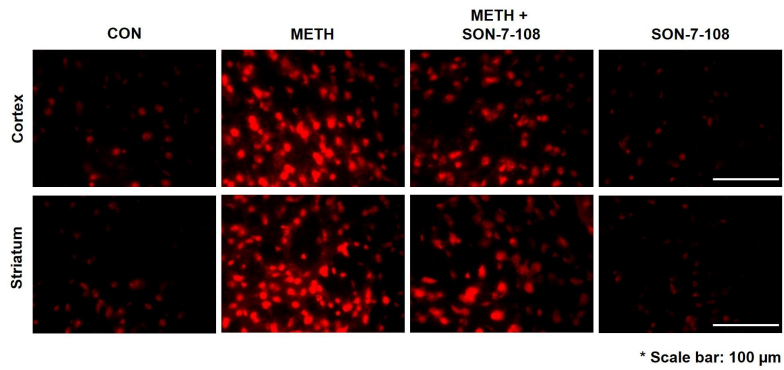
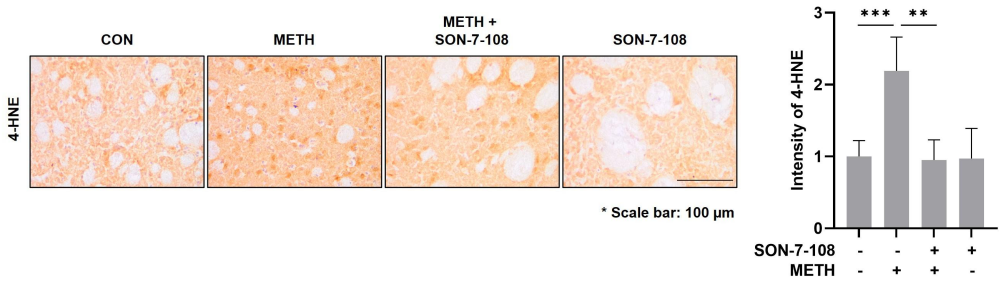


Figure 8. SON-7-108 eliminates METH-induced dopaminergic neuronal damage. Mice were daily intraperitoneally injected with a single dose of 10 mg/kg SON-7-108, and 2 hours after that, mice were injected with 4 administrations of METH at 10 mg/kg every 2 hours. Mice were sacrificed 72 hours after the last injection of METH and striatum sections were used to analyze. (A) Western blot analysis of TH and the quantification normalized to the levels of β -actin using Image J. (B) IHC images of TH signals were obtained from a light microscope and quantified by Image J. (C) Western blot analysis of DAT and the quantification normalized to the levels of GAPDH using Image J. (D) IHC images of DAT signals were obtained from a light microscope and quantified by Image J. Scale bar, 100 μ m. Data is indicated as mean \pm standard deviation (n=5). *: $p < 0.05$, ***: $p < 0.001$. METH: methamphetamine; IHC: immunohistochemistry; TH: tyrosine hydroxylase; DAT: dopamine transporter; CON: control.

A



B



C

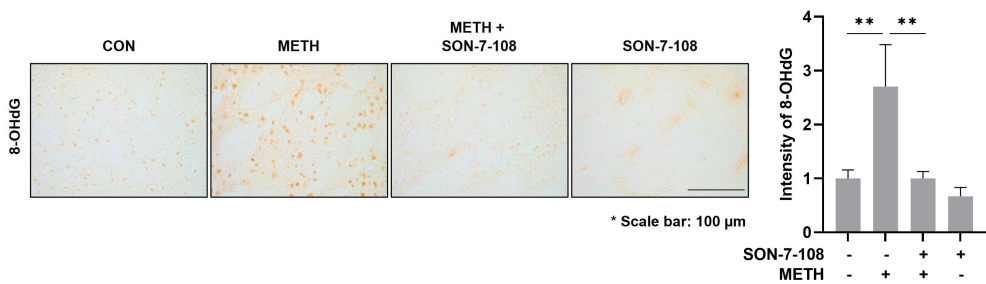
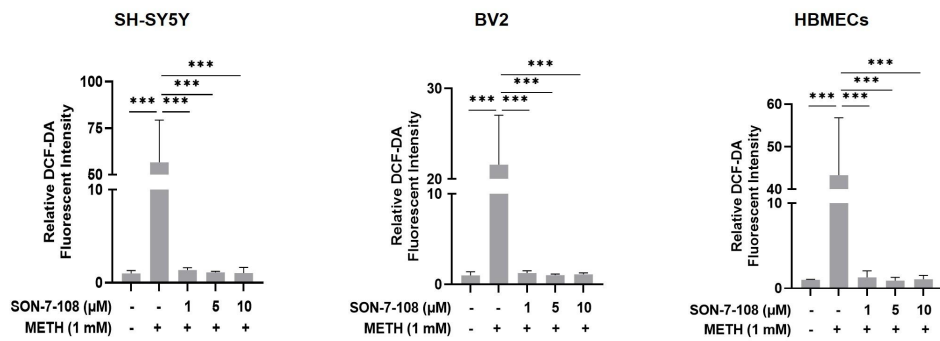
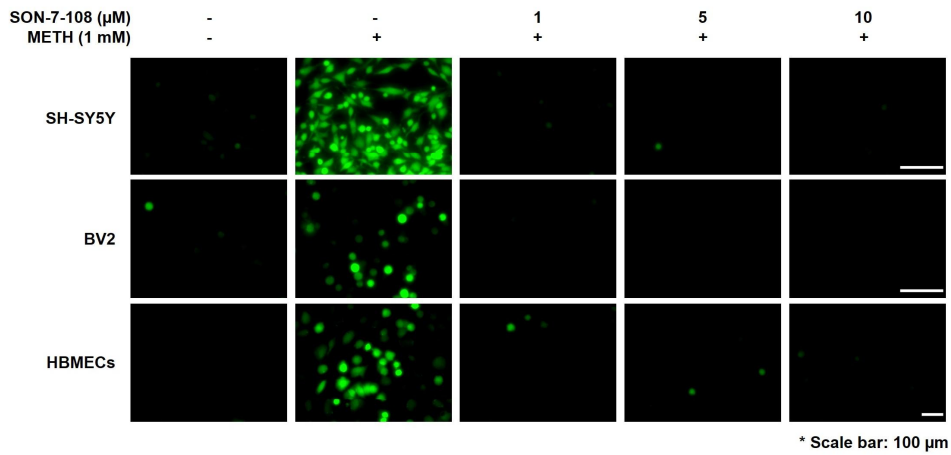


Figure 9. SON-7-108 reduces METH-induced oxidative stress *in vivo*. Mice were daily intraperitoneally injected with a single dose of 10 mg/kg SON-7-108, and 2 hours after that, mice were injected with 4 administrations of METH at 10 mg/kg every 2 hours. Mice were sacrificed 2 hours after the last injection of METH and striatum sections were used to analyze. (A) DHE signals (red) in both cortex and striatum regions representing the superoxide anion levels in tissue were captured using a fluorescent microscope and quantified by Image J. (B) IHC images of 4-HNE signals in striatum region were obtained from a light microscope and quantified by Image J. (C) IHC images of 8-OHdG signals in striatum region were obtained from a light microscope and quantified by Image J. Scale bar, 100 μ m. Data is indicated as mean \pm standard deviation (n=5). *: $p < 0.05$, **: $p < 0.01$, ***: $p < 0.001$. DHE: dihydroethidium; IHC: immunohistochemistry; 4-HNE: 4-hydroxynonenal; 8-OHdG: 8-hydroxy-2'-deoxyguanosine; METH: methamphetamine; CON: control.

A



B

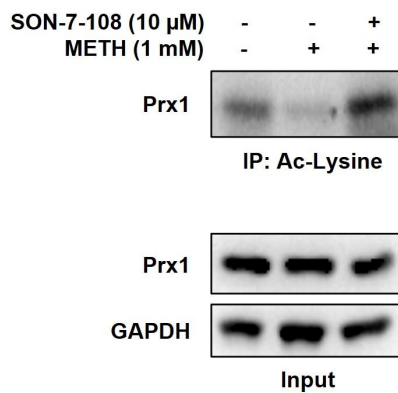


Figure 10. SON-7-108 reduces ROS generation via the prevention of Prx1 deacetylation. Different types of cells were pretreated with SON-7-108 and exposed to METH for 30 minutes. (A) DCF-DA signals representing the ROS levels were captured using a fluorescent microscope and quantified by Image J. Scale bar, 100 μ m. (B) Immunoprecipitation analysis of an acetylated form of Prx1. Data is indicated as mean \pm standard deviation (n=3). ***: $p < 0.001$. DCF-DA: 2',7'-dichlorodihydrofluorescein diacetate; METH: methamphetamine; Prx1: peroxiredoxin-1; Ac-Lysine: acetylated lysine.

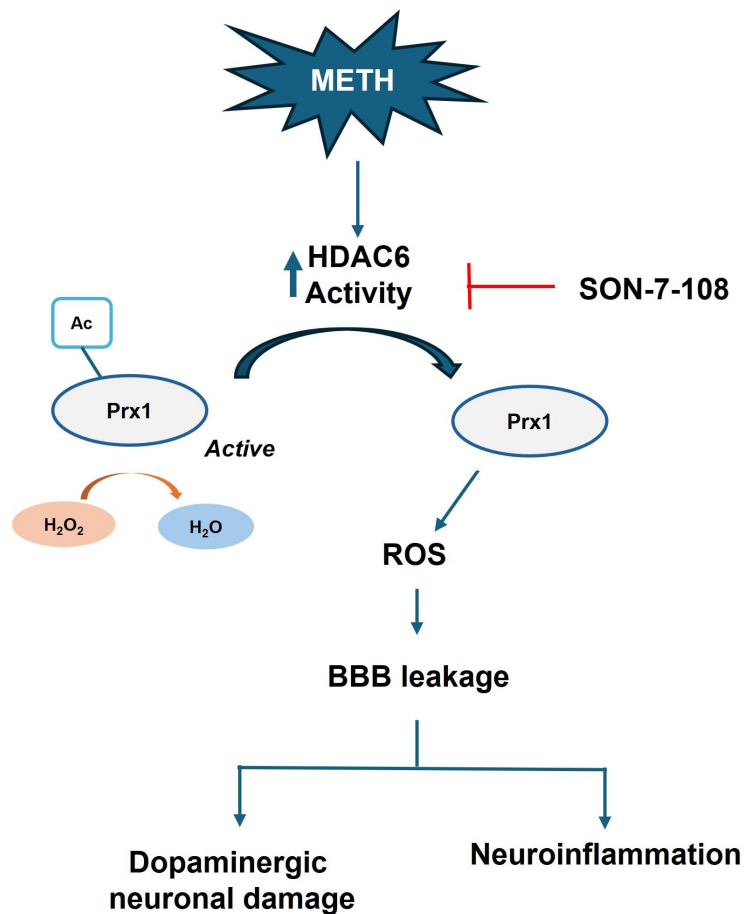


Figure 11. Summary of the study. METH-induced BBB leakage leads to dopaminergic neuronal damage and neuroinflammation via upregulating HDAC6 activity, which reduces the peroxidase function of Prx1. Treatment with SON-7-108 counteracts these effects. METH: methamphetamine; HDAC6: histone deacetylase 6; Prx1: peroxiredoxin-1; Ac: acetyl group.

4. Discussion

METH is a well-known psychostimulant worldwide, with the number of its abusers increasing over time. Being addicted to METH, numerous negative impacts are reported for various failures of organs, including kidneys, livers, lungs, and brain. This study focuses especially on the neurological implications of METH abuse (27–32).

METH is known to reduce DA and serotonin levels, and increase BBB leakage by altering the functions of components that form the BBB (33–37). In addition, METH induces α -tubulin deacetylation, a process facilitated by HDAC6, prompting exploration of HDAC6 inhibitors as potential therapies for METH-induced neurotoxicity (38,39).

Numerous HDAC6 inhibitors have shown the potential to cut down the harmful effects of METH, for instance, reducing memories, behavioral disorders, and neurotoxicity (23–25). However, their efficacy has been challenged by the need for effective penetration through the BBB for optimal therapeutic impact (40,41). Benzimidazole, which is a well-known substance for high lipid-soluble (42), was used to synthesize SON-7-108, the novel HDAC6 inhibitor in this study.

In previous studies, treatment with selective HDAC6 inhibitors resulted in elevated levels of acetyl- α -tubulin (43,44). Similarly, SON-7-108 reduced the HDAC6 activity leading to increased acetyl- α -tubulin levels without affecting the substrate of other HDACs. Both *in vitro* and *in vivo* findings showed inhibitory effects of SON-7-108 against METH-induced α -tubulin deacetylation, suggesting that SON-7-108 is a promising therapeutic compound.

The BBB collapse in the hippocampus of mice typically occurs within 2 hours to 1 day after METH exposure and is restored within 3 days

(45,46). In this study, the mice were examined 2 hours after the last injection of METH, confirming the presence of IgG and neutrophil elastase as markers of BBB compromise, consistent with previous reports. METH-induced ROS production in endothelial cells reduced the expressions of junctional proteins, VE-Cadherin and ZO-1 (47-49). The *in vitro* experiments on HBMECs demonstrated METH-induced redistribution of junctional proteins. However, pretreatment with SON-7-108 mitigated these detrimental effects of METH (Figure 3&4). METH-induced actin stress fiber formation, attributed to increased myosin light chain accumulation, actin-related protein 2/3 complex activation, and matrix metalloproteinase 9 (MMP-9) activity, has also been reported. This disruption further compromised cell monolayer integrity, particularly notable in HBMECs (50-54).

METH also induces neurotoxicity characterized by neuroinflammation and dopaminergic neuronal damage (55). METH exposure leads to the activation of astrocytes and microglia, evidenced by increased expression of their respective protein markers, GFAP and Iba1. Consequently, METH injection causes neuroinflammation with the accumulation of gliosis markers and an increase in pro-inflammatory cytokines levels in mice (56) as shown in Figure 6&7, however, it was attenuated by treatment with SON-7-108.

The involvement of METH in the DA system is well studied. METH reduces TH, an essential enzyme for dopamine synthesis, as well as DAT levels, thus increasing the efflux and reducing the synthesis of DA (13). However, the reduction of TH and DAT by METH was restored by treatment with SON-7-108 (Figure 8).

BBB dysfunction occurs concurrently with METH-induced hyperthermia and excessive ROS production (57,58). ROS is involved in many pathological conditions, and numerous antioxidants are known to

mitigate the harmful effects of METH on the brain. In METH-injected mice, SON-7-108 administration reduced levels of superoxide anions (detected by DHE signals), lipid oxidation (indicated by 4-HNE signals), and DNA damage (measured by 8-OHdG signals) (Figure 9). These findings were supported by the *in vitro* ROS measurement by DCF-DA in the presence of SON-7-108 (Figure 10). These results suggest that HDAC6 plays an important role in the regulation of ROS generation and oxidative stress, therefore, inhibition of HDAC6 would be a therapeutic strategy for ROS-related diseases.

Meanwhile, METH has been reported to cause neuroinflammation through activating pathways of mitogen-activated protein kinase (MAPK) pathways and nuclear factor kappa B (NF- κ B). Various antioxidative substances have shown promise in attenuating METH-induced neuroinflammatory response by preventing ROS generation. Recent investigations into deeper molecular mechanisms have highlighted that HDAC6 plays an important role in counteracting METH-induced negative impacts (59,60). Given its emerging role in neuronal diseases, HDAC6 has garnered attention as a potential therapeutic target for METH-induced neuronal damage.

HDAC6 inhibitors have also shown efficacy in decreasing ROS generation. Prx1 is known as the HDAC6 substrate, and its peroxidase activity is compromised when HDAC6 activity is overexpressed. The reduction in the acetylated form of Prx1 observed in METH-treated cells suggests that METH upregulates HDAC6 activity (Figure 10), resulting in excess ROS generation by decreasing the peroxidase activity of Prx1. Treatment with SON-7-108 counteracted METH-induced Prx1 inactivation. However, this study did not evaluate the specific deacetylation site of Prx1 targeted by HDAC6, which is suggested to be K197 (61). In addition, the mechanism of METH-induced

neuroinflammation was not explored, presenting an opportunity for further study with a new novel HDAC6 inhibitor.

In conclusion, METH cause excessive ROS production by upregulating HDAC6 activity, leading to BBB dysfunction neuroinflammation, and dopaminergic neuronal damage. Treatment with SON-7-108, a novel HDAC6 inhibitor, reduces METH-induced neurotoxicity.

5. Summary

In this study, the protective effect of SON-7-108, a novel benzimidazole-based HDAC6 inhibitor, against METH-induced neurotoxicity was evaluated. METH enhanced ROS generation and caused BBB dysfunction, neuroinflammation, and dopaminergic neuronal damage. By upregulating HDAC6 activity, METH increased the deacetylation of α -tubulin and Prx1, accelerating ROS generation. The application of SON-7-108, a synthesized HDAC6 inhibitor, addressed these issues. It preserved cell monolayer integrity, prevented BBB leakage, reduced the expression of gliosis markers, decreased cytokine production, and mitigated damage to the DA system. SON-7-108 inhibited the deacetylation of α -tubulin and Prx1 caused by METH. Therefore, SON-7-108 could be recognized as a selective HDAC6 inhibitor and a prospective therapeutic approach for METH-induced neuronal damage.

References

1. Cretzmeyer M, Sarrazin MV, Huber DL, Block RI, Hall JA: Treatment of methamphetamine abuse: research findings and clinical directions. *Journal of substance abuse treatment* 2003; 24(3): 267-77.
2. Quinton MS, Yamamoto BK: Causes and consequences of methamphetamine and MDMA toxicity. *The AAPS journal* 2006; 8: E337-47.
3. Bowyer JF, Hanig JP: Amphetamine- and methamphetamine-induced hyperthermia: Implications of the effects produced in brain vasculature and peripheral organs to forebrain neurotoxicity. *Temperature* 2014; 1(3): 172-82.
4. Basova LV, Vien W, Bortell N, Najera JA, Marcondes MCG: Methamphetamine signals transcription of IL1beta and TNFalpha in a reactive oxygen species-dependent manner and interacts with HIV-1 Tat to decrease antioxidant defense mechanisms. *Front Cell Neurosci* 2022; 16: 911060-79.
5. Ahmadi I, Foruozaandeh H: Evaluation the multi-organs toxicity of methamphetamine (METH) in rats. *Toxicologie Analytique et Clinique* 2020; 32(1): 4-11.
6. Volkow ND, Fowler JS, Wang GJ, Shumay E, Telang F, Thanos PK, et al.: Distribution and pharmacokinetics of methamphetamine in the human body: clinical implications. *PLoS One* 2010; 5(12):

E15269-74.

7. Chen L, Ru Q, Xiong Q, Yang J, Xu G, Wu Y: Potential Effects of Nrf2 in Exercise Intervention of Neurotoxicity Caused by Methamphetamine Oxidative Stress. *Oxid Med Cell Longev* 2022; 2022(1): 4445734-48.
8. Knox EG, Aburto MR, Clarke G, Cryan JF, O'Driscoll CM: The blood-brain barrier in aging and neurodegeneration. *Mol Psychiatry* 2022; 27(6): 2659-73.
9. Northrop NA, Yamamoto BK: Methamphetamine effects on blood-brain barrier structure and function. *Front Neurosci* 2015; 9: 69-79.
10. Pang L, Wang Y: Overview of blood-brain barrier dysfunction in methamphetamine abuse. *Biomed Pharmacother* 2023; 161: 114478-87.
11. Sajja RK, Rahman S, Cucullo L: Drugs of abuse and blood-brain barrier endothelial dysfunction: A focus on the role of oxidative stress. *J Cereb Blood Flow Metab* 2016; 36(3): 539-54.
12. Liu L, Zhou X, Shetty S, Hou G, Wang Q, Fu J: HDAC6 inhibition blocks inflammatory signaling and caspase-1 activation in LPS-induced acute lung injury. *Toxicol Appl Pharmacol* 2019; 370: 178-83.
13. Shrestha P, Katila N, Lee S, Seo JH, Jeong JH, Yook S: Methamphetamine induced neurotoxic diseases, molecular mechanism,

- and current treatment strategies. *Biomed Pharmacother* 2022; 154: 113591–608.
14. Hai R, He L, Shu G, Yin G: Characterization of Histone Deacetylase Mechanisms in Cancer Development. *Front Oncol* 2021; 11: 700947–65.
 15. Batchu SN, Brijmohan AS, Advani A: The therapeutic hope for HDAC6 inhibitors in malignancy and chronic disease. *Clin Sci* 2016; 130(12): 987–1003.
 16. Dai Y, Wei T, Shen Z, Bei Y, Lin H, Dai H: Classical HDACs in the regulation of neuroinflammation. *Neurochem Int* 2021; 150: 105182–91.
 17. d'Ydewalle C, Bogaert E, Van Den Bosch L: HDAC6 at the Intersection of Neuroprotection and Neurodegeneration. *Traffic* 2012; 13(6): 771–9.
 18. Simões-Pires C, Zwick V, Nurisso A, Schenker E, Carrupt P-A, Cuendet M: HDAC6 as a target for neurodegenerative diseases: what makes it different from the other HDACs? *Molecular Neurodegeneration* 2013; 8(1): 7–23.
 19. Leng Y, Wu Y, Lei S, Zhou B, Qiu Z, Wang K, et al.: Inhibition of HDAC6 Activity Alleviates Myocardial Ischemia/Reperfusion Injury in Diabetic Rats: Potential Role of Peroxiredoxin 1 Acetylation and Redox Regulation. *Oxid Med Cell Longev* 2018; 2018(1): 9494052–67.

20. Jian W, Wei X, Chen L, Wang Z, Sun Y, Zhu S, et al.: Inhibition of HDAC6 increases acetylation of peroxiredoxin1/2 and ameliorates 6-OHDA induced dopaminergic injury. *Neurosci Lett* 2017; 658: 114–20.
21. Li J, Yu M, Fu S, Liu D, Tan Y: Role of Selective Histone Deacetylase 6 Inhibitor ACY-1215 in Cancer and Other Human Diseases. *Front Pharmacol* 2022; 13: 907981–93.
22. Chae HY, Park SY, Jha S, Gupta SK, Kim M, Ha E, et al.: Design, synthesis, and biological evaluation of bifunctional inhibitors against Hsp90–HDAC6 interplay. *Eur J Med Chem* 2022; 240: 114582–96.
23. Sharma C, Oh YJ, Park B, Lee S, Jeong CH, Lee S, et al.: Development of Thiazolidinedione–Based HDAC6 Inhibitors to Overcome Methamphetamine Addiction. *Int J Mol Sci* 2019; 20(24): 6213–25.
24. Guo Z, Zhang Z, Zhang Y, Wang G, Huang Z, Zhang Q, et al.: Design, synthesis and biological evaluation of brain penetrant benzazepine–based histone deacetylase 6 inhibitors for alleviating stroke–induced brain infarction. *Eur J Med Chem* 2021; 218: 113383–98.
25. Kim B, Jha S, Seo JH, Jeong CH, Lee S, Lee S, et al.: MeBib Suppressed Methamphetamine Self–Administration Response via Inhibition of BDNF/ERK/CREB Signal Pathway in the Hippocampus. *Biomol Ther* 2020; 28(6): 519–26.

26. Choi MA, Park SY, Chae HY, Song Y, Sharma C, Seo YH: Design, synthesis and biological evaluation of a series of CNS penetrant HDAC inhibitors structurally derived from amyloid-beta probes. *Sci Rep* 2019; 9(1): 13187–98.
27. Chang L, Alicata D, Ernst T, Volkow N: Structural and metabolic brain changes in the striatum associated with methamphetamine abuse. *Addiction* 2007; 102: 16–32.
28. Bowyer JF, Ali S: High doses of methamphetamine that cause disruption of the blood-brain barrier in limbic regions produce extensive neuronal degeneration in mouse hippocampus. *Synapse* 2006; 60(7): 521–32.
29. Bowyer JF, Sarkar S, Tranter KM, Hanig JP, Miller DB, O'Callaghan JP: Vascular-directed responses of microglia produced by methamphetamine exposure: indirect evidence that microglia are involved in vascular repair? *J Neuroinflammation* 2016; 13(1): 64–78.
30. Dietrich JB: Alteration of blood-brain barrier function by methamphetamine and cocaine. *Cell Tissue Res* 2009; 336(3): 385–92.
31. Gold MS, Kobeissy FH, Wang KK, Merlo LJ, Bruijnzeel AW, Krasnova IN, et al.: Methamphetamine- and trauma-induced brain injuries: comparative cellular and molecular neurobiological substrates. *Biol Psychiatry* 2009; 66(2): 118–27.
32. Goncalves J, Martins T, Ferreira R, Milhazes N, Borges F, Ribeiro

- CF, et al.: Methamphetamine-induced early increase of IL-6 and TNF- α mRNA expression in the mouse brain. *Ann N Y Acad Sci* 2008; 1139: 103-11.
33. Leita0 RA, Fontes-Ribeiro CA, Silva AP: The effect of parthenolide on methamphetamine-induced blood-brain barrier and astrocyte alterations. *Eur J Clin Invest* 2022; 52(4): E13694-705.
 34. Cliburn RA, Dunn AR, Stout KA, Hoffman CA, Lohr KM, Bernstein AI, et al.: Immunochemical localization of vesicular monoamine transporter 2 (VMAT2) in mouse brain. *J Chem Neuroanat* 2017; 83: 82-90.
 35. Narita M, Suzuki M, Kuzumaki N, Miyatake M, Suzuki T: Implication of activated astrocytes in the development of drug dependence: differences between methamphetamine and morphine. *Ann N Y Acad Sci* 2008; 1141: 96-104.
 36. Shaerzadeh F, Streit WJ, Heysieattalab S, Khoshbouei H: Methamphetamine neurotoxicity, microglia, and neuroinflammation. *J Neuroinflammation* 2018; 15(1): 341-6.
 37. Pimentel E, Sivalingam K, Doke M, Samikkannu T: Effects of Drugs of Abuse on the Blood-Brain Barrier: A Brief Overview. *Front Neurosci* 2020; 14: 513-21.
 38. Fernandes S, Salta S, Summavielle T: Methamphetamine promotes α -tubulin deacetylation in endothelial cells: the protective role of acetyl-l-carnitine. *Toxicol Lett* 2015; 234(2): 131-8.

39. Jayanthi S, McCoy MT, Cadet JL: Epigenetic Regulatory Dynamics in Models of Methamphetamine-Use Disorder. *Genes* 2021; 12(10): 1614–40.
40. Sakloth F, Manouras L, Avrampou K, Mitsi V, Serafini RA, Pryce KD, et al.: HDAC6-selective inhibitors decrease nerve-injury and inflammation-associated mechanical hypersensitivity in mice. *Psychopharmacology* 2020; 237(7): 2139–49.
41. Francelle L, Outeiro TF, Rappold GA: Inhibition of HDAC6 activity protects dopaminergic neurons from alpha-synuclein toxicity. *Sci Rep* 2020; 10(1): 6064–77.
42. Chen G, Liu Z, Zhang Y, Shan X, Jiang L, Zhao Y, et al.: Synthesis and Anti-inflammatory Evaluation of Novel Benzimidazole and Imidazopyridine Derivatives. *ACS Med Chem Lett* 2013; 4(1): 69–74.
43. Zhang WB, Yang F, Wang Y, Jiao FZ, Zhang HY, Wang LW, et al.: Inhibition of HDAC6 attenuates LPS-induced inflammation in macrophages by regulating oxidative stress and suppressing the TLR4-MAPK/NF-kappaB pathways. *Biomed Pharmacother* 2019; 117: 109166–74.
44. Chang Z, Li Y, He W, Liu B, Duan X, Halaweish I, et al.: Inhibition of histone deacetylase 6 restores intestinal tight junction in hemorrhagic shock. *J Trauma Acute Care Surg* 2016; 81(3): 512–9.
45. Turowski P, Kenny BA: The blood-brain barrier and

- methamphetamine: open sesame? *Front Neurosci* 2015; 9: 156-62.
46. Bowyer JF, Tranter KM, Robinson BL, Hanig JP, Faubion MG, Sarkar S: The time course of blood brain barrier leakage and its implications on the progression of methamphetamine-induced seizures. *Neurotoxicology* 2018; 69: 130-40.
 47. Lohr KM, Stout KA, Dunn AR, Wang M, Salahpour A, Guillot TS, et al.: Increased Vesicular Monoamine Transporter 2 (VMAT2; Slc18a2) Protects against Methamphetamine Toxicity. *ACS Chem Neurosci* 2015; 6(5): 790-9.
 48. Gao X, Bayraktutan U: TNF- α evokes blood-brain barrier dysfunction through activation of Rho-kinase and neurokinin 1 receptor. *Immunobiology* 2023; 228(5): 152706-13.
 49. Sweeney MD, Zhao Z, Montagne A, Nelson AR, Zlokovic BV: Blood-Brain Barrier: From Physiology to Disease and Back. *Physiol Rev* 2019; 99(1): 21-78.
 50. Xue Y, He J-T, Zhang K-K, Chen L-J, Wang Q, Xie X-L: Methamphetamine reduces expressions of tight junction proteins, rearranges F-actin cytoskeleton and increases the blood brain barrier permeability via the RhoA/ROCK-dependent pathway. *Biochemical and biophysical research communications* 2019; 509(2): 395-401.
 51. J Young E, B Briggs S, A Miller C: The actin cytoskeleton as a therapeutic target for the prevention of relapse to methamphetamine use. *CNS & Neurological Disorders-Drug Targets (Formerly Current*

Drug Targets-CNS & Neurological Disorders) 2015; 14(6): 731-7.

52. Park M, Kim H-J, Lim B, Wylegala A, Toborek M: Methamphetamine-induced Occludin Endocytosis Is Mediated by the Arp2/3 Complex-regulated Actin Rearrangement. *Journal of Biological Chemistry* 2013; 288(46): 33324-34.
53. Hwang JS, Cha EH, Park B, Ha E, Seo JH: PBN inhibits a detrimental effect of methamphetamine on brain endothelial cells by alleviating the generation of reactive oxygen species. *Arch Pharm Res* 2020; 43(12): 1347-55.
54. Hwang JS, Cha EH, Ha E, Park B, Seo JH: GKT136901 protects primary human brain microvascular endothelial cells against methamphetamine-induced blood-brain barrier dysfunction. *Life Sci* 2020; 256: 117917-27.
55. Ramirez SH, Potula R, Fan S, Eidem T, Papugani A, Reichenbach N, et al.: Methamphetamine disrupts blood-brain barrier function by induction of oxidative stress in brain endothelial cells. *J Cereb Blood Flow Metab* 2009; 29(12): 1933-45.
56. Kim B, Yun J, Park B: Methamphetamine-Induced Neuronal Damage: Neurotoxicity and Neuroinflammation. *Biomol Ther* 2020; 28(5): 381-8.
57. Wells PG, Bhatia S, Drake DM, Miller-Pinsler L: Fetal oxidative stress mechanisms of neurodevelopmental deficits and exacerbation by ethanol and methamphetamine. *Birth Defects Res C Embryo*

Today 2016; 108(2): 108-30.

58. Cunha-Oliveira T, Cristina Rego A, R Oliveira C: Oxidative stress and drugs of abuse: an update. *Mini-Reviews in Organic Chemistry* 2013; 10(4): 321-34.

59. Park JH, Seo YH, Jang JH, Jeong CH, Lee S, Park B: Asiatic acid attenuates methamphetamine-induced neuroinflammation and neurotoxicity through blocking of NF- κ B/STAT3/ERK and mitochondria-mediated apoptosis pathway. *J Neuroinflammation* 2017; 14(1): 240-54.

60. Youn GS, Lee KW, Choi SY, Park J: Overexpression of HDAC6 induces pro-inflammatory responses by regulating ROS-MAPK-NF- κ B/AP-1 signaling pathways in macrophages. *Free Radic Biol Med* 2016; 97: 14-23.

61. Choi H, Kim HJ, Kim J, Kim S, Yang J, Lee W, et al.: Increased acetylation of Peroxiredoxin1 by HDAC6 inhibition leads to recovery of A β -induced impaired axonal transport. *Mol Neurodegener* 2017; 12(1): 23-36.

Protective Effects of HDAC6 Inhibitor on Methamphetamine-Induced Neurotoxicity

Ha Thi Ngoc Vy

Department of Biochemistry
Graduate School

Keimyung University

(Supervised by Professor Ji Hae Seo)

(Abstract)

Methamphetamine (METH) is a highly addictive drug that damages the central nervous system, causing blood-brain barrier (BBB) disruption, neuroinflammation, and dopaminergic neuronal damage. This study investigates the effects of SON-7-108, a new HDAC6 inhibitor, on METH-induced damage. In cell studies, SON-7-108 increased microtubule acetylation, reduced pro-inflammatory cytokine levels, and decreased reactive oxygen species (ROS). In METH-treated mice, SON-7-108 reduced BBB permeability, ROS production, and neuroinflammation, while preserving tyrosine hydroxylase (TH) and dopamine transporter (DAT) levels. These findings suggest that SON-7-108 may be a promising treatment for METH addiction.

Protective Effects of HDAC6 Inhibitor on Methamphetamine-Induced Neurotoxicity

Ha Thi Ngoc Vy

계명대학교 대학원

의학과 생화학 전공

(지도교수 서 지 혜)

(초록)

메스암페타민(METH)은 중독성이 강한 약물로, 중추신경계에 심각한 손상을 초래하며 혈뇌장벽(BBB) 붕괴, 신경 염증, 도파민성 신경 손상을 유발합니다. 본 연구는 METH 유도 손상에 대한 새로운 HDAC6 억제제인 SON-7-108의 효과를 조사합니다. 세포 연구에서 SON-7-108은 미세소관 아세틸화를 증가시키고, 염증성 사이토카인 수치를 감소시키며, 활성 산소종(ROS)을 줄였습니다. METH로 처리한 생쥐에서는 SON-7-108이 BBB 투과성, ROS 생성, 신경 염증을 감소시키고, 티로신 하이드록실화효소(TH)와 도파민 운반체(DAT) 수치를 회복시켰습니다. 이러한 결과는 SON-7-108이 METH 중독에 대한 유망한 치료제가 될 수 있음을 시사합니다.

☐ Biography

1996년 호치민 출생

계명대학교 의과대학 생화학교실 석사학위 대학원생 (현)

☐ Papers and books

None